Electronic Supplementary Material (ESI) for Journal of Materials Chemistry C.

Electric Field- and Light-Responsive Oxadiazole-Bent-Core Polycatenar Liquid Crystals

Mohamed Alaasar,*[a] Ahmed F. Darweesh,[b] Yu Cao,[c] Konstantin Iakoubovskii,*[d] Masafumi Yoshio[d,e]

[a]Institute of Chemistry, Martin Luther University Halle-Wittenberg, 06120 Halle, Germany
[b]Department of Chemistry, Faculty of Science, Cairo University, 12613 Giza, Egypt
[c] Shaanxi International Research Center for Soft Matter, State Key Laboratory for Mechanical Behavior of Materials, Xi'an Jiaotong University, Xi'an 710049, P. R. China
[d]Research Center for Macromolecules & Biomaterials, National Institute for Materials Science, 1-2-1 Sengen, Tsukuba, Ibaraki 305-0047, Japan
[e]Japan Science and Technology Agency, PRESTO, 4-1-8 Honcho, Kawaguchi, Saitama, 332-0012, Japan

Contents

1. Synthesis:

Compounds **3**, **5** and **6** were synthesized using the procedures reported in ref. [S1], while 3,4,5-tris(hexadecyloxy)benzoic acid (**7**) and the azobenzene-based benzoic acid derivatives were synthesized according to the procedure reported in [S2] and [S3], respectively. The synthesis of other intermediates and of the final polycatenar materials is described below.

4-(5-(4-(benzyloxy)phenyl)-1,3,4-oxadiazol-2-yl)phenyl-3,4,5-tris(hexadecyloxy)benzoate (8).

3,4,5-Tris(hexadecyloxy)benzoic acid **7**[S2] (2.0 g, 2.37 mmol, 1.0 equiv.) was heated under reflux with excess thionyl chloride (3.0 mL) and a catalytic amount of *N,N*-dimethylformamide (DMF) for one hour. The excess of thionyl chloride was removed by distillation under reduced pressure. The acid chloride was then dissolved in dry dichloromethane (DCM, 50 mL). To this solution, 5-(4-benzyloxyphenyl)-2-(4-hydroxyphenyl)-1,3,4-oxadiazole **6** (0.81 g, 2.37 mmol, 1.0 equiv.) previously dissolved in DCM (20 mL) was added, followed by addition of triethylamine (0.29 g (0.4 mL), TEA, 2.85 mmol, 1.2 equiv.) and a catalytic amount of pyridine. The solution was then refluxed for 4 hours under an argon atmosphere. After cooling the reaction mixture to the room temperature, it was washed with 10% HCl (2 × 50 mL) and several times with cold water, then extracted with DCM (3 × 50 mL) and finally dried over anhydrous sodium sulfate. The crude residue obtained after removal of solvent was chromatographed on silica gel using hexane/ethylacetate (5:1) to give the pure compound **8**.

8. Colorless solid; m.p. = 83-84 ^{o}C, 2.04 g (1.74 mmol, 74%), $C_{76}H_{116}N_2O_7$; M = 1169.74 g/mol; ^{1}H NMR (400 MHz, $CDCl_3$) δ 8.20 (d, J = 8.8 Hz, 2H, Ar-H), 8.09 (d, J = 8.8 Hz, 2H, Ar-H), 7.46-7.35 (m, 5H, Ar-H), 7.41 (s, 2H, Ar-H), 7.38 (d, J = 8.8 Hz, 2H, Ar-H), 7.12 (d, J = 8.8 Hz, 2H, Ar-H), 5.16 (s, 2H, OCH_2), 4.09- 4.04 (m, 6H, -O$CH_2$$CH_2$), 1.87-1.75 (m, 6H, -$OCH_2CH_2$), 1.59-1.26 (m, 78H, CH_2), 0.89-0.86 (m, 9H, CH_3); ^{13}C NMR (101 MHz, $CDCl_3$) δ = 164.55, 161.57, 153.58, 153.01, 143.34, 136.16, 128.77, 128.69, 128.23, 127.48, 123.31, 122.66, 121.65, 116.55, 115.42, 108.67, 73.61, 70.21, 69.32, 31.91, 30.34, 29.72, 29.69, 29.66, 29.64, 29.62, 29.55, 29.38, 29.36, 29.34, 29.29, 26.07, 26.04, 22.67, 14.09. EA: calc.: C 78.04%, H 10.00%, N 2.39%; found: C 77.95%, H 9.90%, N 2.28%.

4-(5-(4-hydroxyphenyl)-1,3,4-oxadiazol-2-yl)phenyl-3,4,5-tris(hexadecyloxy)benzoate (9)

The benzyl protection group was removed by hydrogenating a solution of the intermediate **8** (1.00 g, 0.92 mmol) in dry tetrahydrofuran (50 mL) at low pressure in the presence of Pd (10% on activated carbon) until no further hydrogen uptake was detectable (overnight). Removal of the catalyst by filtration through Celite and evaporation of the solvent yielded 0.90 g (98%) of **9** as pale yellow solid. m.p. = 89-91 ^{o}C, $C_{69}H_{110}N_2O_7$; M = 1079.62 g/mol; ^{1}H NMR (500 MHz, $CDCl_3$) δ 8.17 (d, J = 8.5 Hz, 2H, Ar-H), 8.01 (d, J = 8.5 Hz, 2H, Ar-H), 7.42 (s, 2H, Ar-H), 7.38 (d, J = 9.0 Hz, 2H, Ar-H), 7.00 (d, J = 9.0 Hz, 2H, Ar-H), 6.98 (s, 1H, OH), 4.09- 4.04 (m, 6H, -OCH_2CH$_2$), 1.86-1.74 (m, 6H, -OCH$_2$$CH_2$), 1.52-1.25 (m, 78H, CH$_2$), 0.89-0.86 (m, 9H, CH$_3$); ^{13}C NMR (126 MHz, $CDCl_3$) δ = 164.76, 163.48, 159.60, 153.60, 153.03, 143.36, 135.77, 128.95, 128.26, 125.49, 123.25, 122.72, 121.54, 116.30, 108.70, 73.66, 69.34, 68.55, 31.92, 31.91, 30.34, 30.31, 29.74, 29.73, 29.70, 29.67, 29.65, 29.63, 29.56, 29.39, 29.36, 29.35, 29.30, 27.81, 26.08, 26.05, 22.67, 22.16, 14.09. EA: calc.: C 76.76%, H 10.27%, N 2.59%; found: C 76.69%, H 10.21%, N 2.48%.

Synthesis of final materials A*n*, A12F$_3$ and A12F$_{23}$

General procedure. The appropriate acid **10*n*** (0.21 mmol, 1.0 equiv.) was heated under reflux with excess thionyl chloride (1.5 mL) and a catalytic amount of DMF for one hour. The excess of thionyl chloride was removed by distillation under reduced pressure. The acid chloride was then dissolved in dry DCM (20 mL). To this solution, 4-(5-(4-hydroxyphenyl)-1,3,4-oxadiazol-2-yl)phenyl-3,4,5-tris(hexadecyloxy)benzoate **9** (0.21 mmol, 1.0 equiv.) previously dissolved in DCM (10 mL) was added, followed by addition of TEA (0.25 mmol, 1.2 equiv.) and a catalytic amount of pyridine. The solution was then refluxed for 4 hours under an argon atmosphere. After cooling the reaction mixture to the room temperature, it was washed with 10% HCl (2 × 20 mL) and several times with cold water, then extracted with DCM (3 × 20 mL) and finally dried over anhydrous sodium sulfate. The crude residue obtained after removal of solvent was chromatographed on silica gel using $CHCl_3$/ethylacetate (4:1) as eluent. The orange material obtained after removing the solvent was recrystallized from a 1:3 chloroform:ethanol mixture to give the final materials. The analytical data are as follows:

4-(5-(4-((4-((4-(Octyloxy)phenyl)diazenyl)benzoyl)oxy)phenyl)-1,3,4-oxadiazol-2-yl)phenyl-3,4,5-tris(hexadecyloxy)benzoate

A8. Orange crystals; 255 mg (0.180 mmol, 86%), $C_{90}H_{134}N_4O_9$; *M* = 1416.04 g/mol; ^{1}H NMR (500 MHz, $CDCl_3$) δ 8.35 (d, *J* = 8.5 Hz, 2H, Ar-H), 8.26-8.22 (m, 4H, Ar-H), 8.00-7.96 (m, 4H, Ar-H), 7.47 (d, *J* = 8.5 Hz, 2H, Ar-H), 7.42 (s, 2H, Ar-H), 7.41 (d, *J* = 9.0 Hz, 2H, Ar-H), 7.03 (d, *J* = 9.0 Hz, 2H, Ar-H), 4.09- 4.04 (m, 8H, -O*CH*$_2$CH$_2$), 1.85-1.74 (m, 8H, -OCH$_2$*CH*$_2$), 1.61-1.26 (m, 88H, CH_2), 0.91-0.86 (m, 12H, CH_3); ^{13}C NMR (126 MHz, $CDCl_3$) δ = 164.54, 164.21, 164.10, 164.04, 162.58, 156.01, 153.79, 153.61, 153.03, 146.86, 143.38, 131.66, 131.30, 129.83, 128.42, 128.38, 125.44, 125.36, 123.29, 122.75, 122.64, 122.60, 114.86, 108.70, 73.62, 69.34, 68.49, 31.91, 31.79, 30.35, 29.74, 29.73, 29.70, 29.67, 29.65, 29.63, 29.56, 29.39, 29.36, 29.35, 29.33, 29.31, 29.21, 29.16, 26.08, 26.05, 26.00, 22.67, 22.64, 14.09, 14.08. EA: calc.: C 76.34%, H 9.54%, N 3.96%; found: C 76.24%, H 9.42%, N 3.80%.

4-(5-(4-((4-((4-(Decyloxy)phenyl)diazenyl)benzoyl)oxy)phenyl)-1,3,4-oxadiazol-2-yl)phenyl-3,4,5-tris(hexadecyloxy)benzoate

A10. Orange crystals; 272 mg (0.189 mmol, 90%), $C_{92}H_{138}N_4O_9$; *M* = 1444.10 g/mol; ^{1}H NMR (500 MHz, $CDCl_3$) δ 8.35 (d, *J* = 9.0 Hz, 2H, Ar-H), 8.26-8.22 (m, 4H, Ar-H), 8.00-7.96 (m, 4H, Ar-H), 7.47 (d, *J* = 8.5 Hz, 2H, Ar-H), 7.42 (s, 2H, Ar-H), 7.41 (d, *J* = 9.0 Hz, 2H, Ar-H), 7.03 (d, *J* = 9.0 Hz, 2H, Ar-H), 4.09- 4.04 (m, 8H, -O*CH*$_2$CH$_2$), 1.87-1.74 (m, 8H, -OCH$_2$*CH*$_2$), 1.51-1.25 (m, 92H, CH_2), 0.90-0.86 (m, 12H, CH_3); ^{13}C NMR (126 MHz, $CDCl_3$) δ = 164.57, 164.22, 162.47, 156.00, 153.81, 153.52, 153.03, 146.86, 143.34, 131.30, 129.83, 128.43, 128.38, 125.35, 122.75, 122.64, 122.60, 121.56, 121.46, 114.86, 108.70, 73.62, 69.34, 68.49, 31.91, 31.88, 30.35, 29.73, 29.70, 29.67, 29.65, 29.63, 29.55, 29.54, 29.39, 29.36, 29.35, 29.30, 29.15, 26.08, 26.05, 26.00, 22.67, 14.09. EA: calc.: C 76.52%, H 9.63%, N 3.88%; found: C 76.44%, H 9.52%, N 3.81%.

4-(5-(4-((4-((4-(Dodecyloxy)phenyl)diazenyl)benzoyl)oxy)phenyl)-1,3,4-oxadiazol-2-yl)phenyl-3,4,5-tris(hexadecyloxy)benzoate

A12. Orange crystals; 270 mg (0.183 mmol, 87%), $C_{94}H_{142}N_4O_9$; *M* = 1472.15 g/mol; ^{1}H NMR (500 MHz, $CDCl_3$) δ 8.35 (d, *J* = 8.5 Hz, 2H, Ar-H), 8.26-8.22 (m, 4H, Ar-H), 8.00-7.96 (m, 4H, Ar-H), 7.47 (d, *J* = 8.5 Hz, 2H, Ar-H), 7.42 (s, 2H, Ar-H), 7.41 (d, *J* = 9.0 Hz, 2H, Ar-H), 7.03 (d,

J = 9.0 Hz, 2H, Ar-H), 4.09- 4.04 (m, 8H, -O*CH*$_2$CH$_2$), 1.86-1.73 (m, 8H, -OCH$_2$*CH*$_2$), 1.49-1.26 (m, 96H, CH$_2$), 0.89-0.86 (m, 12H, CH$_3$); ^{13}C NMR (126 MHz, CDCl$_3$) δ = 164.55, 164.22, 164.02, 162.57, 156.03, 153.66, 153.53, 153.03, 146.86, 143.29, 131.30, 129.83, 128.42, 128.38, 125.35, 123.29, 122.75, 122.64, 122.60, 121.46, 114.86, 108.70, 73.62, 69.34, 68.49, 31.91, 31.88, 30.35, 29.73, 29.70, 29.67, 29.65, 29.63, 29.55, 29.54, 29.39, 29.36, 29.35, 29.30, 29.15, 26.08, 26.05, 26.00, 22.67, 14.09. EA: calc.: C 76.69%, H 9.72%, N 3.81%; found: C 76.61%, H 9.62%, N 3.75%.

4-(5-(4-((4-((4-(Tetradecyloxy)phenyl)diazenyl)benzoyl)oxy)phenyl)-1,3,4-oxadiazol-2-yl)phenyl-3,4,5-tris(hexadecyloxy)benzoate

A14. Orange crystals; 261 mg (0.174 mmol, 83%), $C_{96}H_{146}N_4O_9$; *M* = 1500.20 g/mol; ^{1}H NMR (500 MHz, CDCl$_3$) δ 8.35 (d, *J* = 8.5 Hz, 2H, Ar-H), 8.25-8.22 (m, 4H, Ar-H), 8.00-7.96 (m, 4H, Ar-H), 7.46 (d, *J* = 9.0 Hz, 2H, Ar-H), 7.42 (s, 2H, Ar-H), 7.41 (d, *J* = 9.0 Hz, 2H, Ar-H), 7.03 (d, *J* = 9.0 Hz, 2H, Ar-H), 4.09- 4.04 (m, 8H, -O*CH*$_2$CH$_2$), 1.86-1.75 (m, 8H, -OCH$_2$*CH*$_2$), 1.60-1.26 (m, 100H, CH$_2$), 0.89-0.86 (m, 12H, CH$_3$); ^{13}C NMR (126 MHz, CDCl$_3$) δ = 164.54, 164.21, 164.04, 162.57, 156.02, 153.78, 153.61, 153.03, 146.86, 143.38, 131.30, 129.83, 128.42, 128.37, 125.34, 123.29, 122.75, 122.64, 122.60, 121.61, 121.46, 114.85, 108.70, 73.62, 69.33, 68.48, 31.93, 31.92, 30.36, 29.75, 29.73, 29.70, 29.68, 29.67, 29.66, 29.65, 29.63, 29.58, 29.57, 29.55, 29.39, 29.37, 29.35, 29.31, 29.16, 26.09, 26.06, 26.00, 22.68, 14.10. EA: calc.: C 76.86%, H 9.81%, N 3.73%; found: C 76.81%, H 9.70%, N 3.65%.

4-(5-(4-((4-((4-(Hexadecyloxy)phenyl)diazenyl)benzoyl)oxy)phenyl)-1,3,4-oxadiazol-2-yl)phenyl-3,4,5-tris(hexadecyloxy)benzoate

A16. Orange crystals; 256 mg (0.167 mmol, 80%), $C_{98}H_{150}N_4O_9$; *M* = 1528.26 g/mol; ^{1}H NMR (500 MHz, CDCl$_3$) δ 8.35 (d, *J* = 8.5 Hz, 2H, Ar-H), 8.26-8.22 (m, 4H, Ar-H), 8.00-7.96 (m, 4H, Ar-H), 7.47 (d, *J* = 8.5 Hz, 2H, Ar-H), 7.42 (s, 2H, Ar-H), 7.41 (d, *J* = 8.5 Hz, 2H, Ar-H), 7.03 (d, *J* = 8.5 Hz, 2H, Ar-H), 4.09- 4.04 (m, 8H, -O*CH*$_2$CH$_2$), 1.87-1.73 (m, 8H, -OCH$_2$*CH*$_2$), 1.52-1.26 (m, 104H, CH$_2$), 0.89-0.86 (m, 12H, CH$_3$); ^{13}C NMR (126 MHz, CDCl$_3$) δ = 164.55, 164.16, 164.02, 162.45, 155.91, 153.80, 153.61, 153.03, 146.89, 143.31, 131.30, 129.83, 128.43, 128.38, 125.35, 123.25, 122.75, 122.64, 122.60, 121.61, 121.43, 114.86, 108.70, 73.62, 69.34, 68.49, 31.91, 31.92, 30.35, 29.75, 29.73, 29.70, 29.68, 29.67, 29.66, 29.65, 29.63, 29.58, 29.57, 29.55, 29.39, 29.37, 29.35, 29.31, 29.15, 26.08, 26.05, 25.99, 22.68, 14.09. EA: calc.: C 77.02%, H 9.89%, N 3.67%; found: C 76.89%, H 9.77%, N 3.58%.

4-(5-(4-((4-((4-(Octadecyloxy)phenyl)diazenyl)benzoyl)oxy)phenyl)-1,3,4-oxadiazol-2-yl)phenyl-3,4,5-tris(hexadecyloxy)benzoate

A18. Orange crystals; 277 mg (0.178 mmol, 85%), $C_{100}H_{154}N_4O_9$; *M* = 1556.31 g/mol; ^{1}H NMR (500 MHz, $CDCl_3$) δ 8.35 (d, *J* = 9.0 Hz, 2H, Ar-H), 8.26-8.22 (m, 4H, Ar-H), 8.00-7.96 (m, 4H, Ar-H), 7.47 (d, *J* = 9.0 Hz, 2H, Ar-H), 7.42 (s, 2H, Ar-H), 7.41 (d, *J* = 9.0 Hz, 2H, Ar-H), 7.03 (d, *J* = 9.0 Hz, 2H, Ar-H), 4.09- 4.04 (m, 8H, -O*CH*$_2$CH$_2$), 1.87-1.74 (m, 8H, -OCH$_2$*CH*$_2$), 1.59-1.26 (m, 108H, CH_2), 0.89-0.86 (m, 12H, CH_3); ^{13}C NMR (126 MHz, $CDCl_3$) δ = 164.54, 164.21, 164.10, 164.04, 162.58, 156.02, 153.79, 153.61, 153.03, 146.86, 143.38, 131.30, 129.83, 128.42, 128.38, 125.35, 123.29, 122.75, 122.64, 122.60, 121.61, 121.45, 114.85, 108.70, 73.62, 69.34, 68.49, 31.91, 30.35, 29.74, 29.73, 29.70, 29.67, 29.65, 29.63, 29.58, 29.56, 29.55, 29.39, 29.36, 29.35, 29.31, 29.15, 26.08, 26.05, 25.99, 22.68, 14.09. EA: calc.: C 77.17%, H 9.97%, N 3.60%; found: C 77.10%, H 9.83%, N 3.50%.

4-(5-(4-((4-((4-(Dodecyloxy)-3-fluorophenyl)diazenyl)benzoyl)oxy)phenyl)-1,3,4-oxadiazol-2-yl)phenyl-3,4,5-tris(hexadecyloxy)benzoate

A12F$_3$. Orange crystals; 250 mg (0.168 mmol, 80%), $C_{94}H_{141}FN_4O_9$; *M* = 1490.41 g/mol; ^{1}H NMR (500 MHz, $CDCl_3$) δ 8.36 (d, *J* = 8.5 Hz, 2H, Ar-H), 8.26-8.22 (m, 4H, Ar-H), 8.00 (d, *J* = 9.0 Hz, 2H, Ar-H), 7.83 (ddd, *J* = 8.5, 2.0, 1.0 Hz, Ar-H, 1H), 7.75 (dd, *J* = 12.0, 2.5 Hz, Ar-H, 1H), 7.47 (d, *J* = 8.5 Hz, 2H, Ar-H), 7.42 (s, 2H, Ar-H), 7.41 (d, *J* = 9.0 Hz, 2H, Ar-H), 7.10 (t, *J* = 9.0 Hz, Ar-H, 1H), 4.15-4.04 (m, 8H, -O*CH*$_2$CH$_2$), 1.89-1.75 (m, 8H, -OCH$_2$*CH*$_2$), 1.50-1.25 (m, 96H, CH_2), 0.89-0.86 (m, 12H, CH_3); ^{13}C NMR (126 MHz, $CDCl_3$) δ = 164.55, 164.13, 164.03, 155.63, 153.89, 153.79, 153.57, 153.03, 151.91, 150.85, 150.76, 143.38, 131.33, 130.26, 128.44, 128.38, 123.88, 123.28, 122.76, 122.62, 121.65, 121.44, 119.48, 113.45, 108.69, 107.92, 73.62, 69.57, 69.34, 31.91, 31.90, 30.35, 29.73, 29.70, 29.67, 29.65, 29.63, 29.56, 29.52, 29.39, 29.36, 29.35, 29.33, 29.32, 29.30, 29.05, 26.08, 26.05, 25.88, 22.67, 14.09. ^{19}F NMR (470 MHz, $CDCl_3$) δ = -132.51 (dd, *J* =11.7, 8.4 Hz). EA: calc.: C 75.76%, H 9.54%, N 3.76%; found: C 75.60%, H 9.43%, N 3.68%.

4-(5-(4-((4-((4-(Dodecyloxy)-2,3-difluorophenyl)diazenyl)benzoyl)oxy)phenyl)-1,3,4-oxadiazol-2-yl)phenyl 3,4,5-tris(hexadecyloxy)benzoate

A12F$_{23}$. Orange crystals; 244 mg (0.161 mmol, 77%), $C_{94}H_{140}F_2N_4O_9$; *M* = 1508.13 g/mol; ^{1}H NMR (500 MHz, $CDCl_3$) δ 8.36 (d, *J* = 8.0 Hz, 2H, Ar-H), 8.26-8.22 (m, 4H, Ar-H), 8.03 (d, *J* = 8.5 Hz, 2H, Ar-H), 7.62-7.59 (m, Ar-H, 1H), 7.47 (d, *J* = 8.5 Hz, 2H, Ar-H), 7.42 (s, 2H, Ar-H),

7.41 (d, J = 8.5 Hz, 2H, Ar-H), 6.84-6.80 (m, Ar-H, 1H), 4.16-4.04 (m, 8H, -O$CH_2$$CH_2$), 1.88-1.75 (m, 8H, -OCH$_2$$CH_2$), 1.51-1.25 (m, 96H, CH_2), 0.89-0.86 (m, 12H, CH_3); ^{13}C NMR (126 MHz, $CDCl_3$) δ = 164.54, 164.11, 164.06, 164.00, 155.77, 153.79, 153.54, 153.03, 143.39, 135.52, 131.68, 131.34, 130.64, 128.43, 128.38, 123.28, 123.19, 123.01, 122.75, 122.61, 121.68, 111.98, 108.70, 108.48, 73.62, 70.09, 69.34, 31.91, 31.90, 30.35, 29.73, 29.70, 29.67, 29.65, 29.63, 29.61, 29.55, 29.50, 29.39, 29.36, 29.35, 29.33, 29.30, 29.28, 29.04, 26.08, 26.05, 25.81, 22.67, 14.09. ^{19}F NMR (470 MHz, $CDCl_3$) δ -145.89 (ddd, J = 18.8, 7.5, 2.0 Hz), -157.98 (ddd, J = 18.8, 7.5, 2.4 Hz). EA: calc.: C 74.86%, H 9.36%, N 3.71%; found: C 74.75%, H 9.31%, N 3.63%.

2. Representative NMR spectra

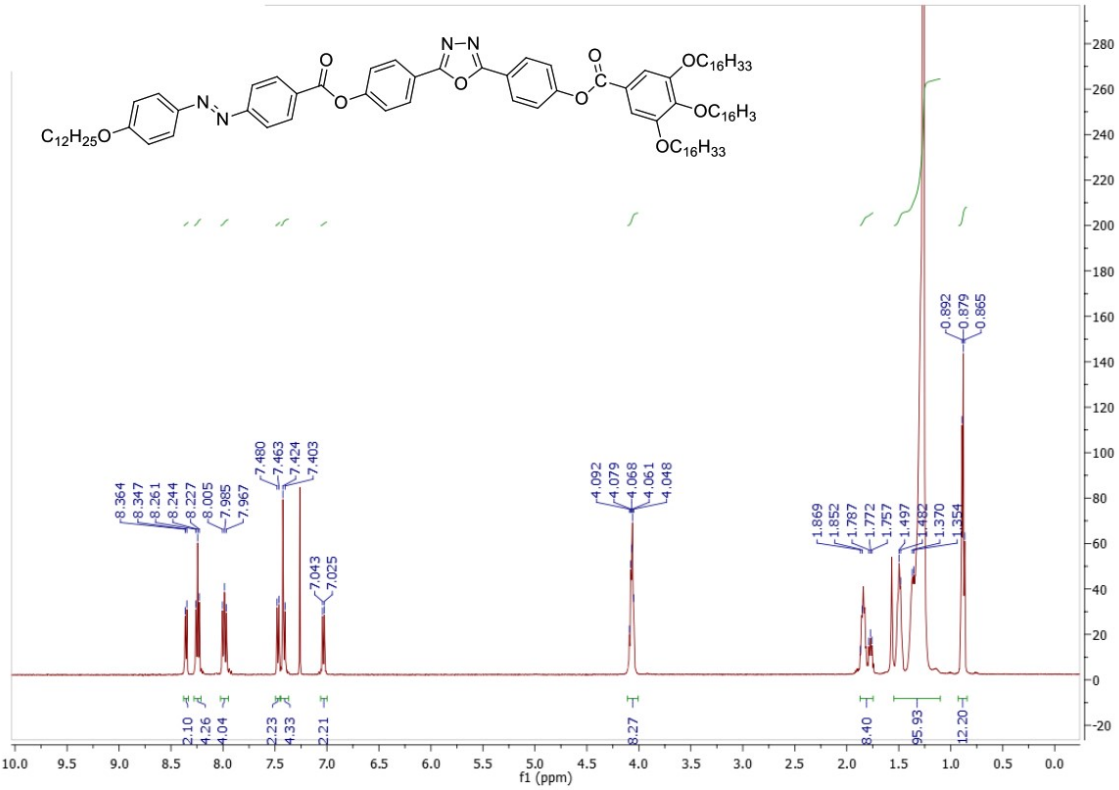

Figure S1. ^{1}H-NMR spectrum of **A12** in $CDCl_3$.

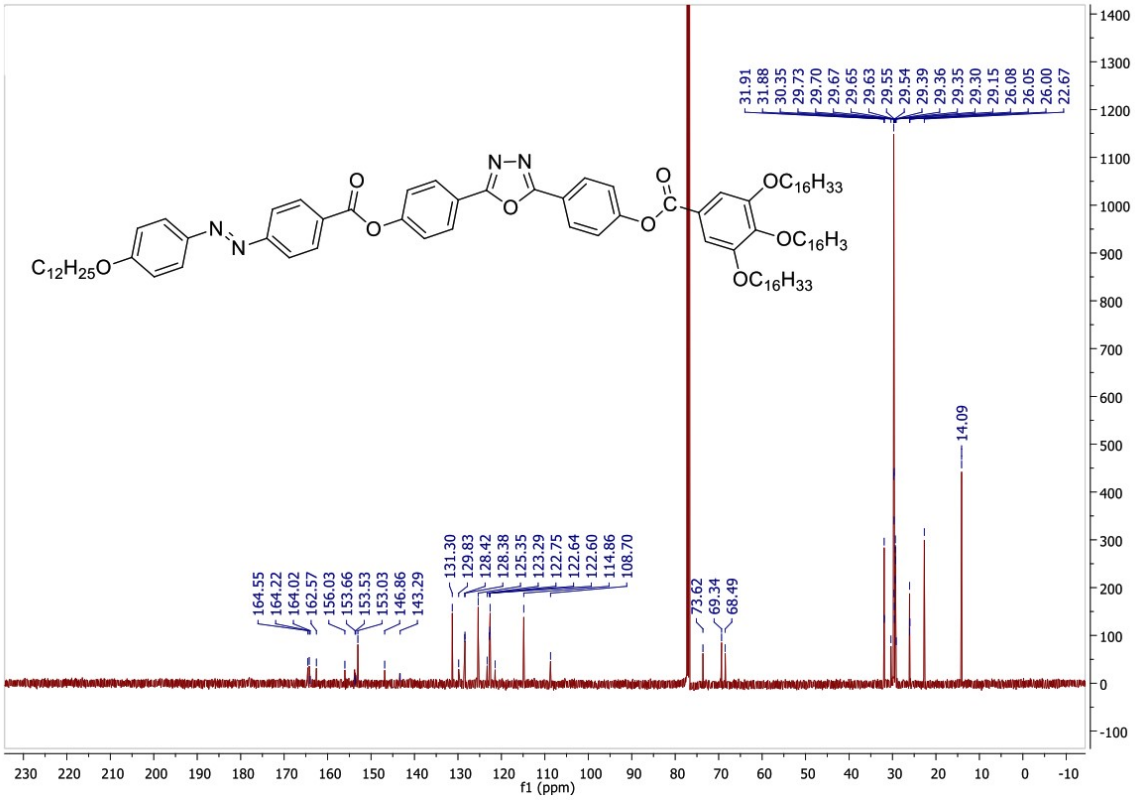

Figure S2. ^{13}C-NMR spectrum of **A12** in $CDCl_3$.

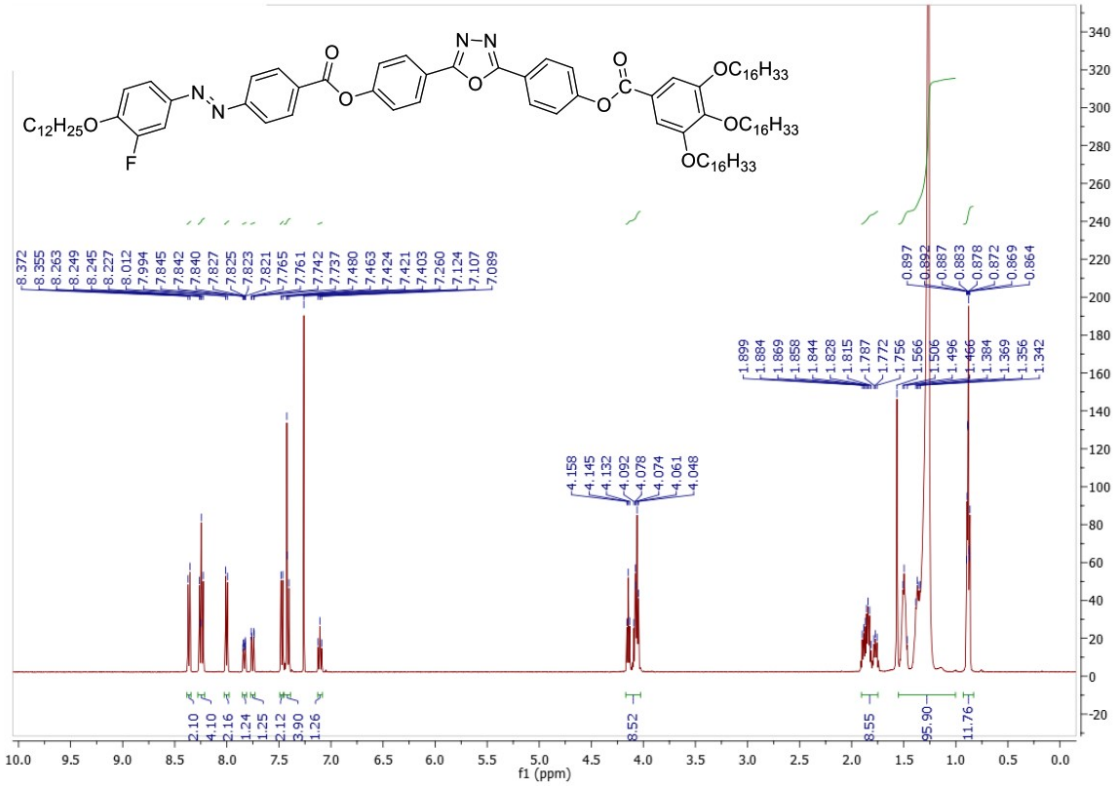

Figure S3. ^{1}H-NMR spectrum of **A12F$_3$** in $CDCl_3$.

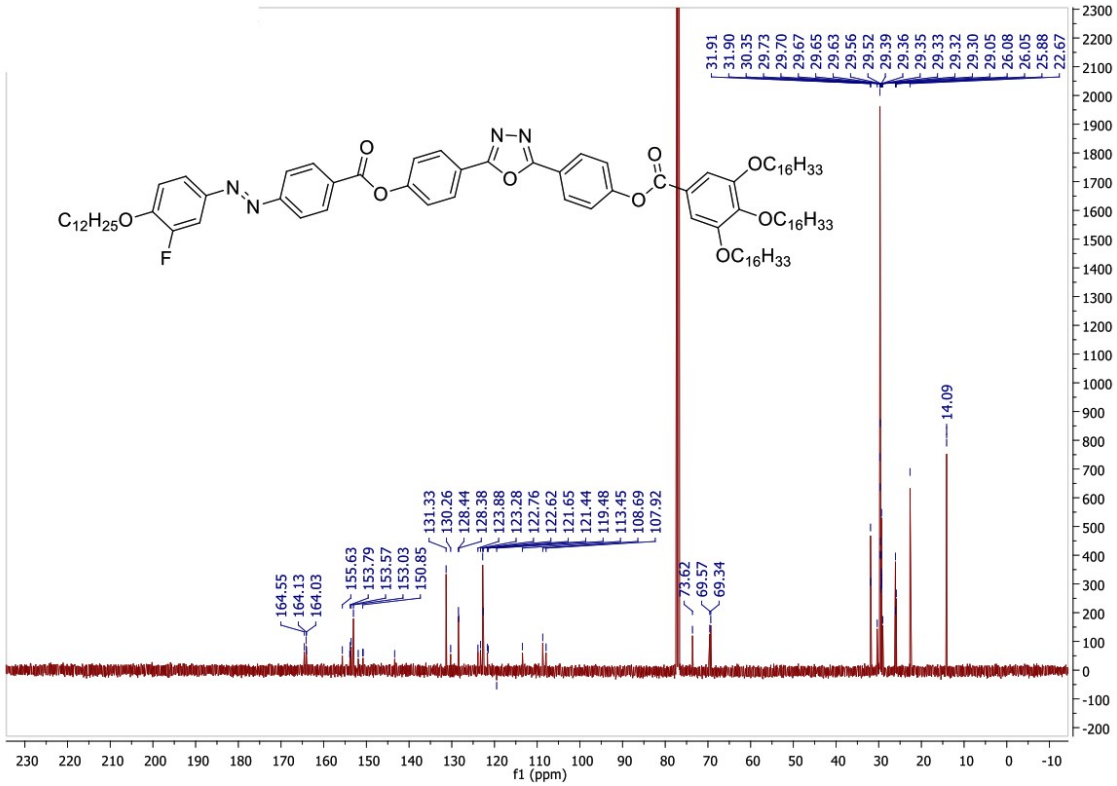

Figure S4. ^{13}C-NMR spectrum of **A12F$_3$** in $CDCl_3$.

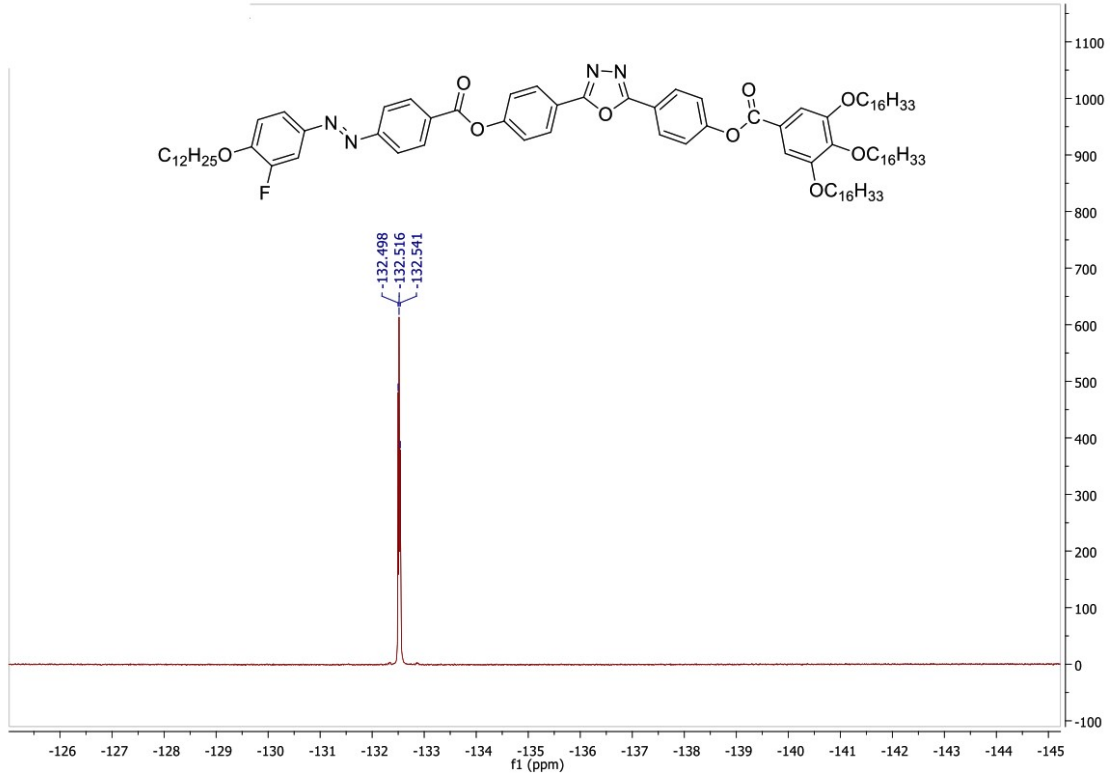

Figure S5. ^{19}F-NMR spectrum of **A12F$_3$** in $CDCl_3$.

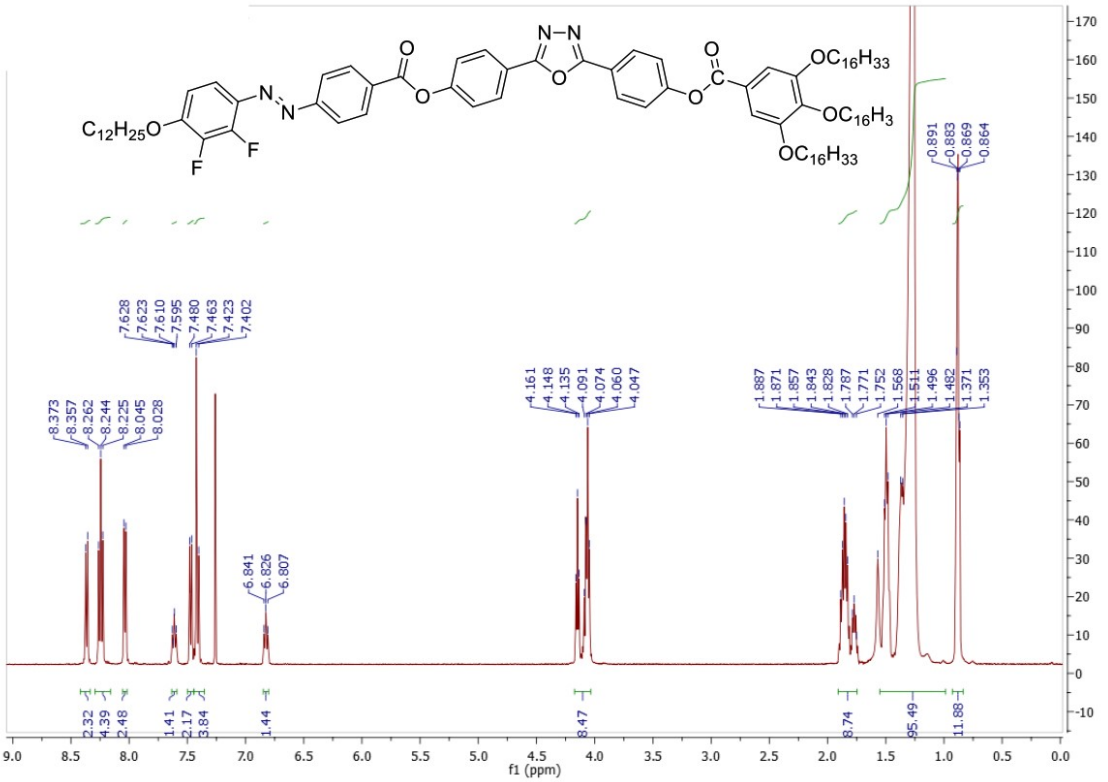

Figure S6. ^{1}H-NMR spectrum of **A12F$_{23}$** in $CDCl_3$.

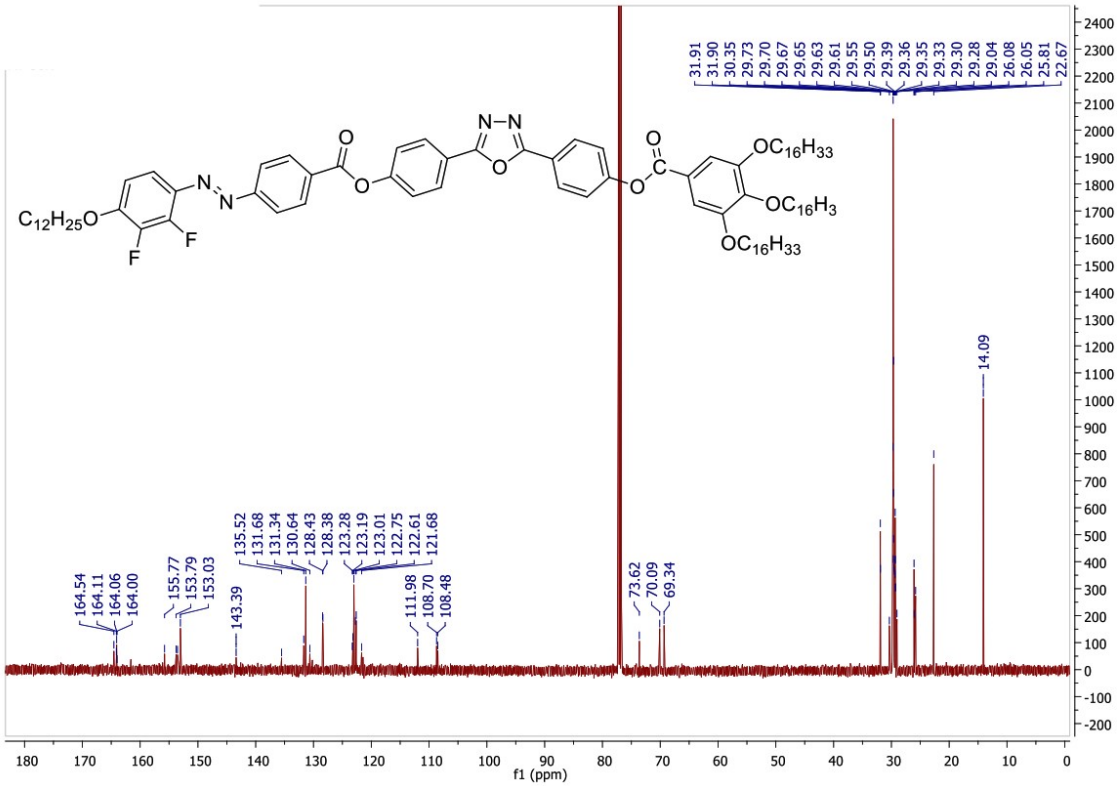

Figure S7. ^{13}C-NMR spectrum of **A12F$_{23}$** in $CDCl_3$.

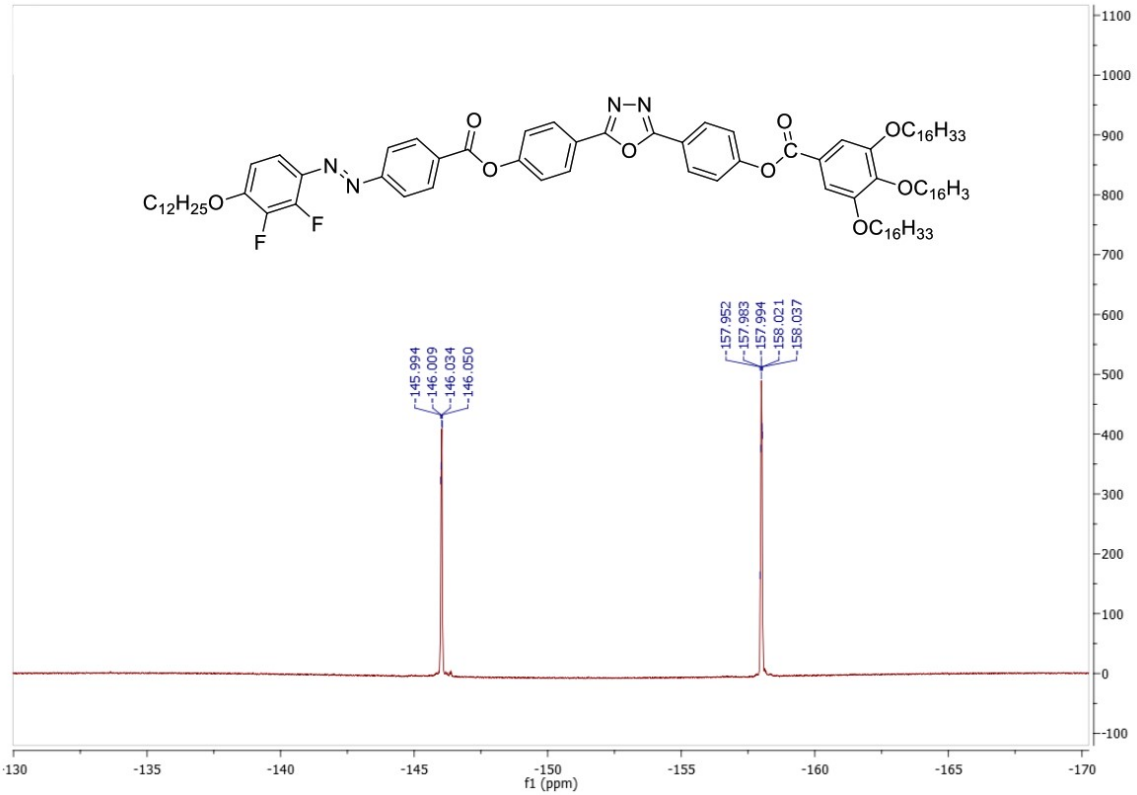

Figure S8. ^{19}F-NMR spectrum of **A12F$_{23}$** in $CDCl_3$.

3. Phase characterization by optical microscopy and DSC

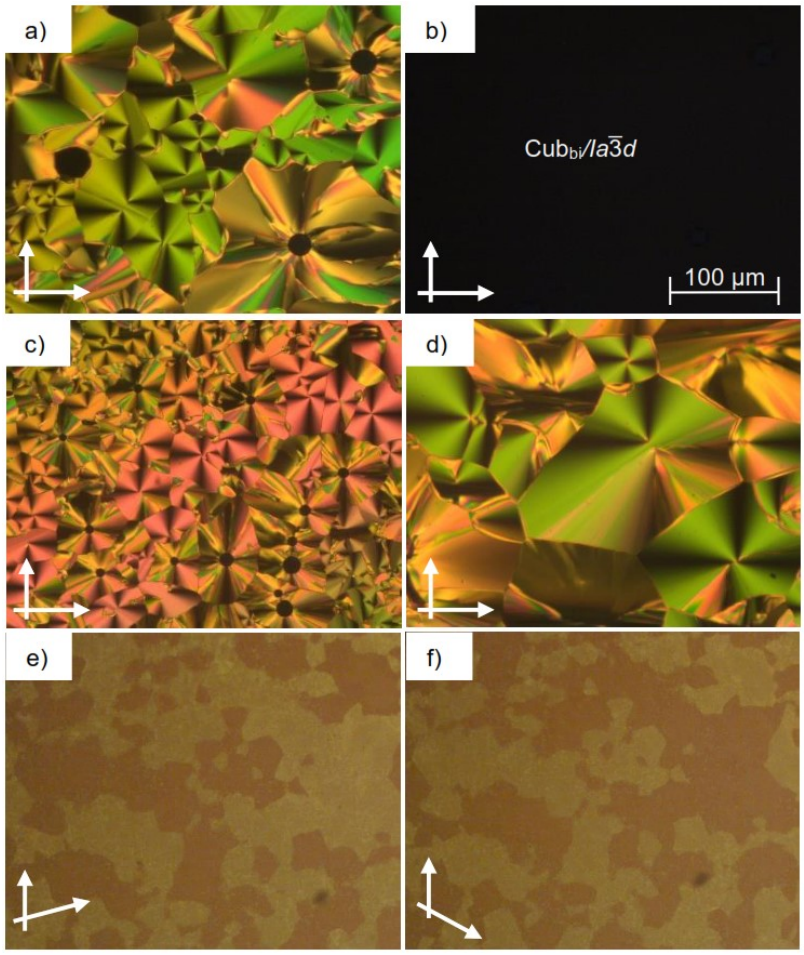

Figure S9. Cross-polarized optical micrographs observed on cooling in: a) Col_{hex} phase of compound **A8** at 111 °C; b) the achiral Cub_{bi}/$Ia\bar{3}d$ phase of **A8** at 108 °C; c) Col_{hex} phase of **A10** at 135 °C; d) Col_{hex} phase of **A16** at 130°C; e,f) chiral crystalline phase of $\mathbf{A12F_{23}}$ after 15 ° rotation one of the analyzers clockwise (e) or anticlockwise (f). The scale bar for all images is given in b).

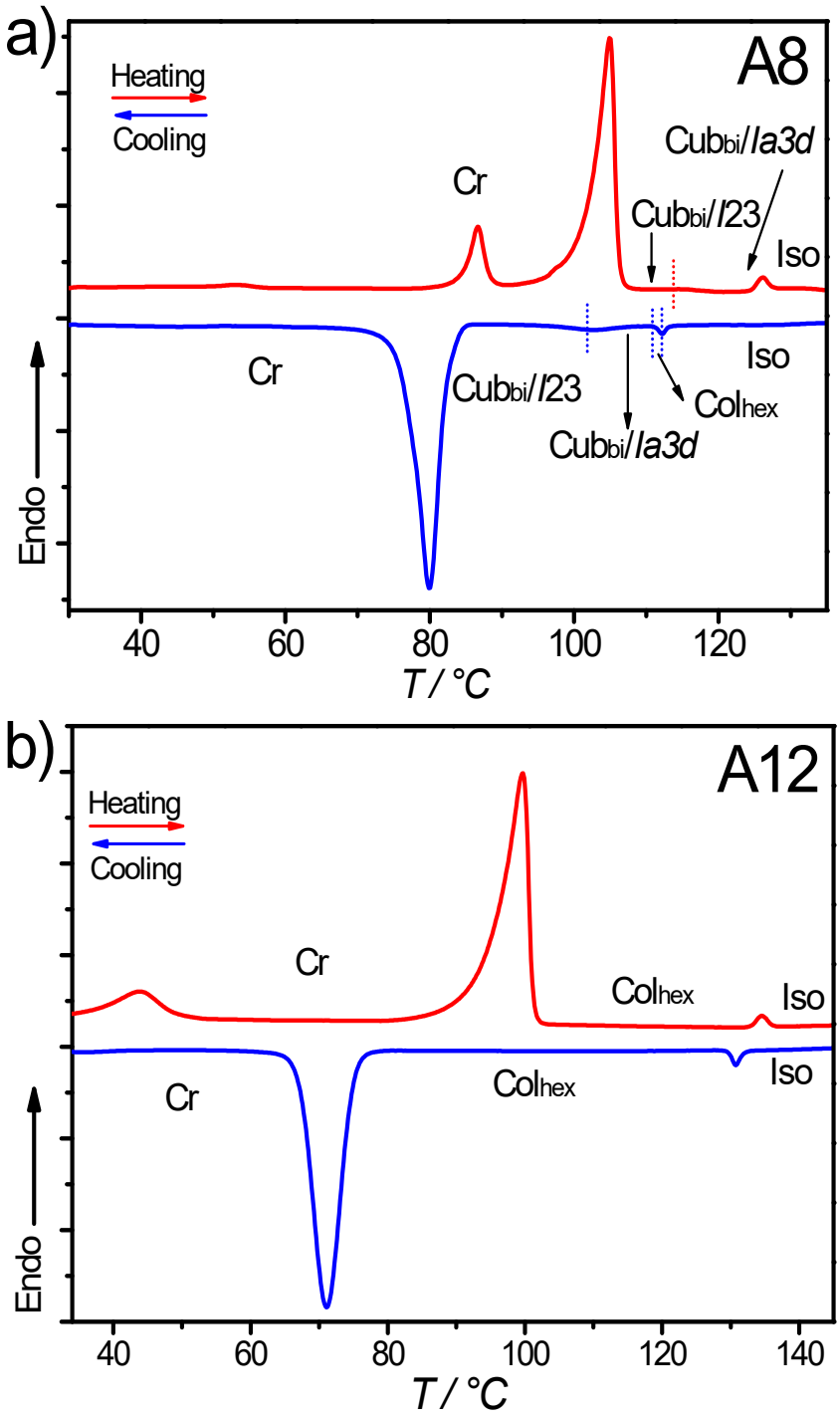

Figure S10. DSC heating and cooling traces at a rate of 10 K min^{-1} for compounds: a) **A8** and b) **A12**.

4. SAXS data

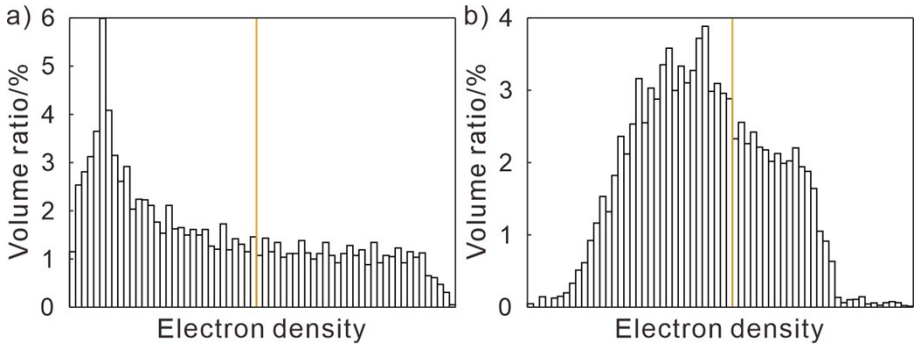

Figure S11. Histograms of electron density for the a) $Cub_{bi}/Ia\bar{3}d$ and b) $Cub_{bi}/I23$ phases of **A8**.

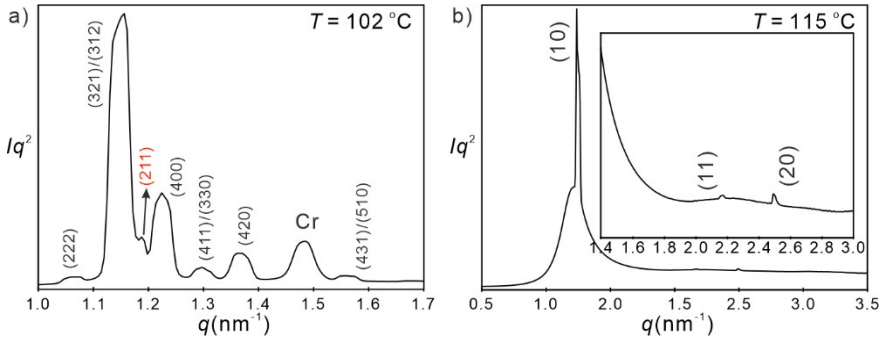

Figure S12. a) SAXS pattern of **A8** with three phases, recorded upon heating at 102 °C. The (211) peak of $Cub_{bi}/Ia\bar{3}d$ phase is marked by red color, $Cub_{bi}/I23$ indexes are black, and the crystalline peak is labelled as Cr; b) The hexagonal columnar phase of **A8** at 115 °C upon cooling.

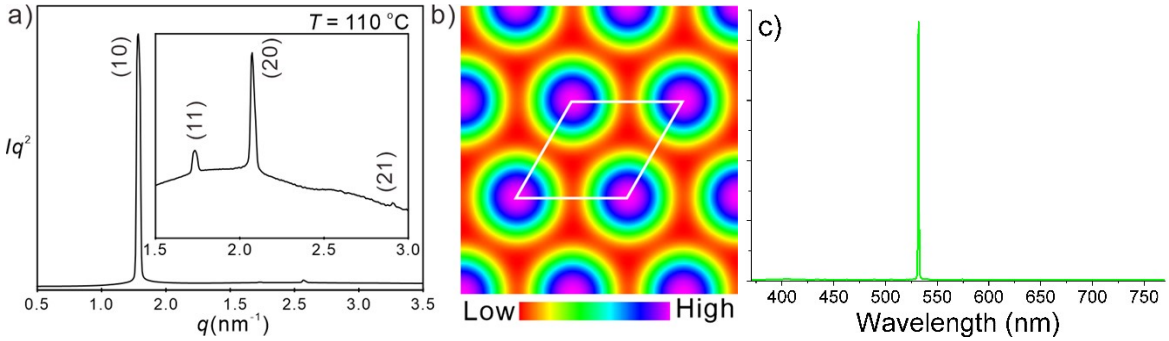

Figure S13. SAXS diffractogram of the Col hexagonal *p6mm* phase with indexation at 110 °C upon heating and b) electron density map; high electron density is in purple and low electron density is in red. Lattice is in white. Panel c) shows a room-temperature second-harmonic generation spectrum recorded from **A12F$_{23}$**.

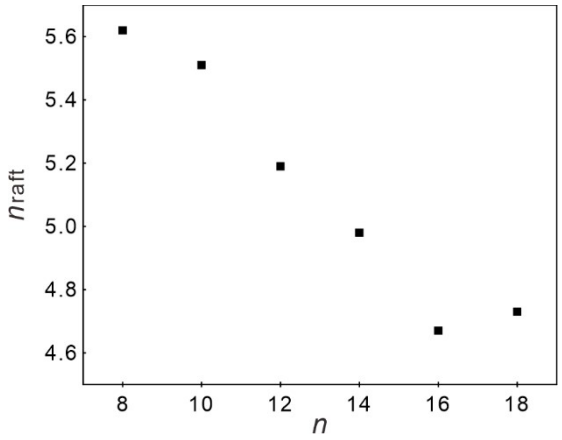

Figure S14. The *n* dependence of the number of molecules per raft n_{raft} for hexagonal columnar phase of **A*n*** at 110 °C except for **A8**, which is at 115 °C.

Table S1 Experimental and calculated *d*-spacings, relative integrated intensities, and phases used in the reconstruction of electron densities for the $Ia\bar{3}d$ cubic phase of **A8** at 114 ºC upon heating. All intensities are Lorentz and multiplicity corrected.

(hkl)	$d_{obs.}$ (nm)	$d_{cal.}$ (nm)	*intensity*	*phase*
(211)	5.24	5.24	100.0	π
(220)	4.55	4.55	32.7	π
(321)	3.43	3.43	0.02	0
(400)	3.21	3.21	1.3	π
(332)	2.75	2.75	0.1	π
(422)	2.63	2.62	0.3	0
(431)	2.52	2.52	0.03	π
a_{cub} = 12.83 nm				

Table S2 Experimental and calculated *d*-spacings, relative integrated intensities, and phases used in the reconstruction of electron densities for the *p6mm* columnar phase of **A8** at 115 ºC upon cooling. All intensities are Lorentz and multiplicity corrected.

(hk)	$d_{obs.}$ (nm)	$d_{cal.}$ (nm)	*intensity*	*phase*
(10)	5.04	5.04	100	0
(11)	2.90	2.91	0.2	π
(20)	2.51	2.52	0.4	π
a_{hex} = 5.82 nm				

Table S3 Experimental and calculated *d*-spacings, relative integrated intensities, and phases used in the reconstruction of electron densities for the *I*23 cubic phase of **A8** at 100 ºC upon cooling. All intensities are Lorentz and multiplicity corrected. Note that for this non-centrosymmetric group, the phase can take arbitrary values between 0 and 2π. A model-dependent simulation was carried in ref. [S4] for this structure to determine the phases.

(hkl)	$d_{obs.}$ (nm)	$d_{cal.}$ (nm)	*intensity*	*phase*
(211)	8.27	8.26	0.05	-0.97π
(220)	7.16	7.16	0.09	/
(301)	6.40	6.40	0.3	0
(222)	5.84	5.84	4.3	-0.24π
(321)	5.41	5.41	23.3	-0.91π
(312)	5.41	5.41	51.4	-0.59π
(400)	5.07	5.06	100.0	0
(330)	4.78	4.77	6.1	0
(411)	4.78	4.77	6.5	-0.81π
(420)	4.53	4.53	9.6	0
(332)	4.31	4.32	0.07	/
(422)	4.14	4.13	0.5	-0.66π
(431)	3.97	3.97	0.6	/
(510)			/	/
(521)	3.70	3.70	0.08	/
(433)	3.47	3.47	0.3	/
(530)			0.3	/
(442)	3.38	3.37	0.08	/
(600)			0.3	/
(532)	3.28	3.28	0.2	/
(611)			0.5	/
(541)	3.13	3.12	0.07	/
(631)	2.99	2.98	0.05	/

(444)	2.92	2.92	0.2	/
(640)	2.82	2.81	0.04	/
(552)	2.76	2.75	0.2	/
(633)			0.2	/
(721)			0.1	/
(651)	2.57	2.57	0.02	/
(732)			0.02	/
a_{cub} = 20.24 nm				

Table S4 Experimental and calculated *d*-spacings, relative integrated intensities, and phases used in the reconstruction of electron densities for the *p6mm* columnar phase of **A10** at 110 ºC upon cooling. All intensities are Lorentz and multiplicity corrected.

(hk)	$d_{obs.}$ (nm)	$d_{cal.}$ (nm)	*intensity*	*phase*
(10)	5.04	5.04	100	0
(11)	2.91	2.91	0.4	π
(20)	2.52	2.52	1.0	π
(21)	1.90	1.91	0.02	π
a_{hex} = 5.82 nm				

Table S5 Experimental and calculated *d*-spacings, relative integrated intensities, and phases used in the reconstruction of electron densities for the *p6mm* columnar phase of **A12** at 110 ºC upon cooling. All intensities are Lorentz and multiplicity corrected.

(hk)	$d_{obs.}$ (nm)	$d_{cal.}$ (nm)	*intensity*	*phase*
(10)	4.94	4.94	100	0
(11)	2.85	2.85	0.01	π
(20)	2.47	2.47	0.04	π
a_{hex} = 5.70 nm				

Table S6 Experimental and calculated *d*-spacings, relative integrated intensities, and phases used in the reconstruction of electron densities for the *p6mm* columnar phase of **A14** at 110 ºC upon cooling. All intensities are Lorentz and multiplicity corrected.

(hk)	$d_{obs.}$ (nm)	$d_{cal.}$ (nm)	*intensity*	*phase*
(10)	4.88	4.88	100	0
(11)	2.81	2.82	0.2	π
(20)	2.44	2.44	0.8	π
(21)	1.84	1.85	0.01	π
a_{hex} = 5.64 nm				

Table S7 Experimental and calculated *d*-spacings, relative integrated intensities, and phases used in the reconstruction of electron densities for the *p6mm* columnar phase of **A16** at 110 ºC upon cooling. All intensities are Lorentz and multiplicity corrected.

(hk)	$d_{obs.}$ (nm)	$d_{cal.}$ (nm)	*intensity*	*phase*
(10)	4.77	4.77	100	0
(11)	2.75	2.76	0.1	π
(20)	2.39	2.39	0.8	π
a_{hex} = 5.51 nm				

Table S8 Experimental and calculated *d*-spacings, relative integrated intensities, and phases used in the reconstruction of electron densities for the *p6mm* columnar phase of **A18** at 110 ºC upon cooling. All intensity values are Lorentz and multiplicity corrected.

(hk)	$d_{obs.}$ (nm)	$d_{cal.}$ (nm)	*intensity*	*phase*
(10)	4.85	4.85	100	0
(11)	2.80	2.80	0.1	π
(20)	2.42	2.42	0.7	π
a_{hex} = 5.60 nm				

Table S9 Experimental and calculated *d*-spacings, relative integrated intensities, and phases used in the reconstruction of electron densities for the *p6mm* columnar phase of **A12F$_3$** at 110 ºC upon cooling. All intensities are Lorentz and multiplicity corrected.

(hk)	$d_{obs.}$ (nm)	$d_{cal.}$ (nm)	*intensity*	*phase*
(10)	4.76	4.76	100	0
(11)	2.72	2.75	0.1	π
(20)	2.36	2.38	0.7	π
a_{hex} = 5.50 nm				

Table S10 Experimental and calculated *d*-spacings, relative integrated intensities, and phases used in the reconstruction of electron densities for the *p6mm* columnar phase of **A12F$_{23}$** at 110 ºC upon cooling. All intensities are Lorentz and multiplicity corrected.

(hk)	$d_{obs.}$ – spacing (nm)	$d_{cal.}$ – spacing (nm)	*intensity*	*phase*
(10)	4.66	4.66	100	0
(11)	2.69	2.69	0.1	π
(20)	2.33	2.33	0.7	π
a_{hex} = 5.38 nm				

Table S11 Distributions of electron density in alkyl and aromatic parts of compounds **A*n***

		Number of electrons	Volume (nm^3)	Electron density (e/nm^3)	*V* %
A8	alkyl chain	452	1.047	432	64.0
	aromatic core	322	0.590	546	36.0
A10	alkyl chain	468	1.081	433	64.7
	aromatic core	322	0.590	546	35.3
A12	alkyl chain	484	1.115	434	65.4
	aromatic core	322	0.590	546	34.6
A14	alkyl chain	500	1.149	435	66.1
	aromatic core	322	0.590	546	33.9
A16	alkyl chain	516	1.183	436	66.7
	aromatic core	322	0.590	546	33.3
A18	alkyl chain	532	1.217	437	67.3
	aromatic core	322	0.590	546	32.7
A12F$_3$	alkyl chain	484	1.115	434	65.1
	aromatic core	330	0.597	553	34.9
A12F$_{23}$	alkyl chain	484	1.115	434	64.9
	aromatic core	338	0.602	561	35.1

5. Impedance analysis for $A12F_{23}$

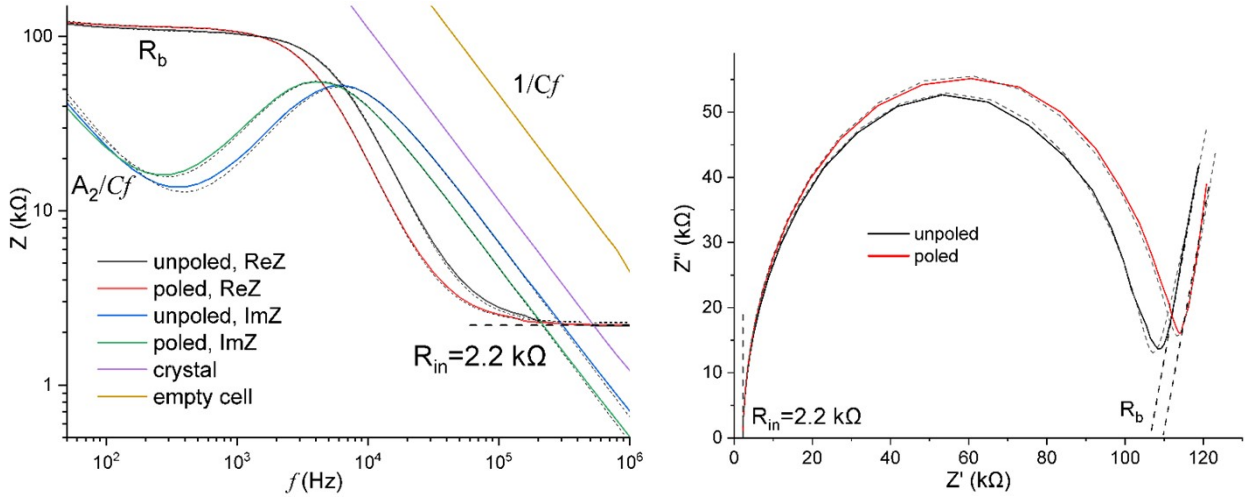

Figure S15. Impedance plots for **$A12F_{23}$** in a 4 μm cell at 118 °C before and after poling at 5 V/μm. Dashed lines show fitting curves. Comparison with the empty cell yields the following dielectric constants: ε = 4 (crystal, 0.1 MHz), ε = 7 (LC), ε = 10 (poled LC).

Impedance data were fitted with the following general formula:

$$Z = \frac{R_{in} - j\cdot 2\pi f C_{in} R_{in}^2}{1 + (2\pi f R_{in} C_{in})^2} + \frac{R_b - j\cdot 2\pi f C_b R_b^2}{1 + (2\pi f R_b C_b)^2} + \frac{A_1}{(jf)^{\alpha}} \qquad (1)$$

Here the first term describes an RC circuit resulting from thin interfacial layers between the LC and the contacts, the second term is the bulk RC circuit, and the last term is a constant-phase element. The exponent α is usually close to 1, and hence the last term becomes jA_2/f, where f is frequency. The *c*onstant-phase element vanishes at high frequencies, not just because of its $1/f$ behavior, but because the constant A_2 must be small to fit the low-f part.

For non-zero constants, equation 1 has the following frequency behavior:

Re(Z) = Z': R_{in}+R_b at low f and 1/fC at high f.

Im(Z) = Z'': A_2/f at low f and 1/fC at high f.

However, for $C_{in} \sim 0$, Z' at high f behaves not as 1/fC, but saturates at the value R_{in}.

Fit parameters:

before poling: R_{in} = 2.30±0.05 kΩ, R_b = 105±3 kΩ, C_b = 245±6 pF, α = 0.96

after poling: R_{in} = 2.30±0.05 kΩ, R_b = 110±3 kΩ, C_b = 350±6 pF, α = 0.94

empty cell: C = 35 pF

Here, similar to some previous studies, we observe a large capacitance and hence a large dielectric constant in a ferroelectric LC. Such results were rebutted in ref. [S5], where after detailed analysis the authors concluded that the large dielectric constant originates not from the LC, but from the thin interfacial layers between the LC and the electrodes. Such interfacial layers were indeed observed in **A12F$_{23}$**, but eliminated after a few poling/heating cycles. This is seen in **Figure S16** that reveals the high-frequency saturation of Z' after cycling. Hence this study justifies the assignment of large dielectric constant to a ferroelectric LC.

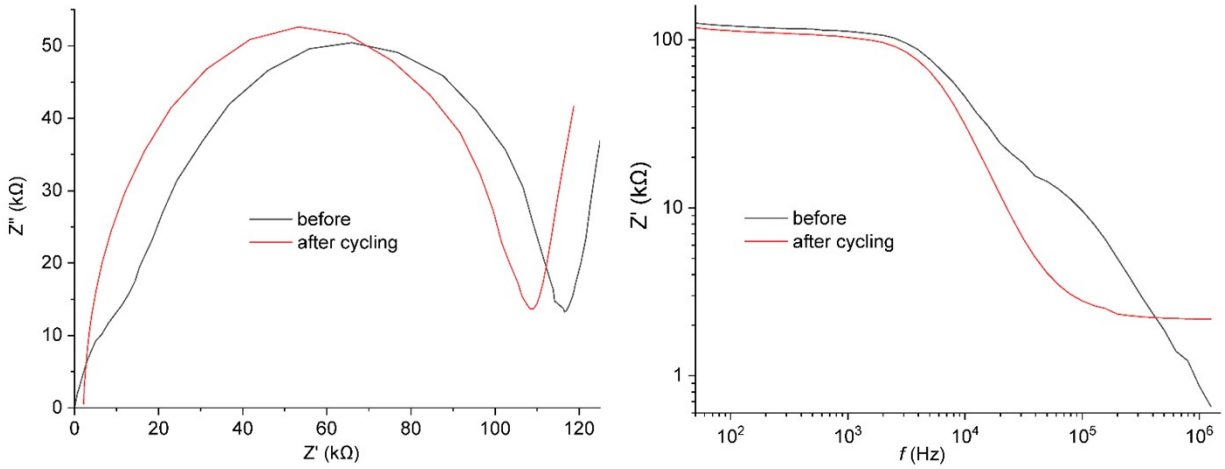

Figure S16. Impedance plots of the same **A12F$_{23}$** sample before and after elimination of the interfacial capacitance. The elimination is obvious from the different number of semicircles in the Nyquist plot (left), and from the different high-frequency behavior of Z' (right).

6. UV-induced amorphization

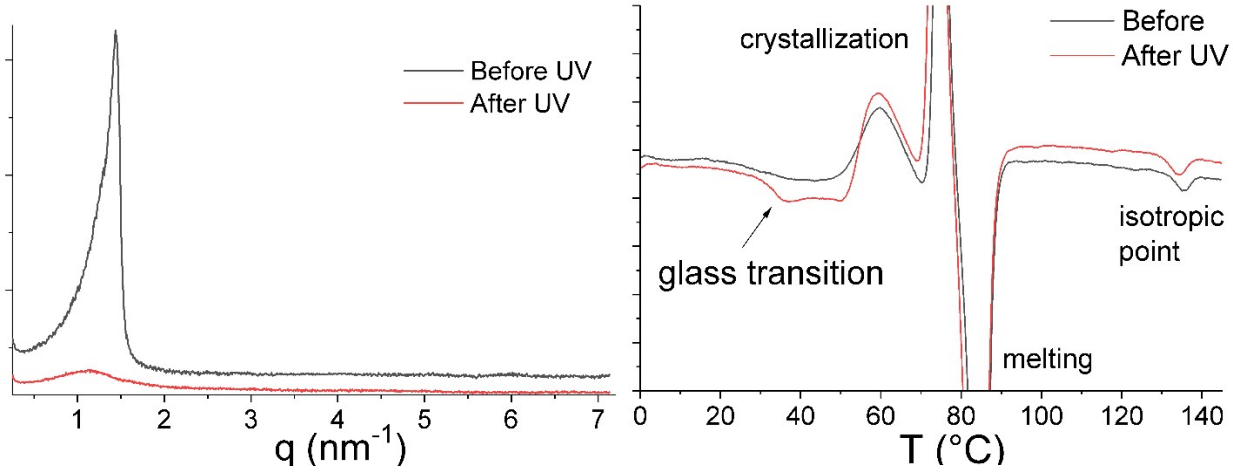

Figure S17. Left: Room-temperature SAXS patterns from **A12** before and after irradiation with 350 nm light. Right: DSC curves from **A18** before and after UV irradiation.

The UV-induced amorphization, which was suggested by polarized optical microscopy, was confirmed by SAXS and DSC. For SAXS experiments, we have squeezed a piece of molten material between two pieces of kapton tape, and then separated them by peeling. This resulted in two large-area thin samples (~5 μm × 2 mm × 5 mm), which were almost completely amorphized by a few-second irradiation with 350 nm light (40 mW cm^{-2}) in the LC phase, as demonstrated by the SAXS patterns in the left part of **Figure S17**. The relatively large width of the main LC peak before irradiation is an collimation artefact resulting from the large area of the sample, which was required to accumulate a measurable signal after irradiation; this artefact originates from the finite size of detector, which is illuminated by a slightly divergent X-ray beam.

Due to technical limitations in sample preparation and lower sensitivity of DSC compared to SAXS, DSC measurements were performed on a thicker sample (~20 μm). Hence, a crystallization peak was reduced, but not erased, by the UV illumination with the same parameters. Nevertheless, a glass transition shoulder did appear at ~ 32 ºC, providing an additional confirmation to the UV-induced amorphization.

7. Overview of phases in polycatenar molecules

We have derived the overall relationship between molecular length and phases by combining data from our present and previous studies.[S6-S8] With the increase of alkyl volume (represented as total number of carbon atoms), the phase transition sequence is Sm – $Ia\bar{3}d$ – $I23$ – Tet_{bi} – $Ia3d$ – $p6mm$.

Table S12 Alkyl chain size and mesophase types of compounds **B*m*/*n*** and **C*m*/*n***

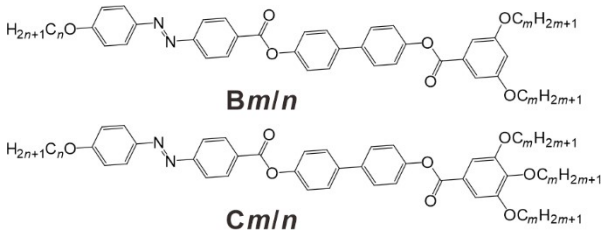

Cpd.	*m*	*n*	Carbon atoms in alkyl chains	Phases
B	6	4	16	Sm
	6	5	17	Sm
	6	6	18	Sm
	6	7	19	Sm – $Ia\bar{3}d$
	6	8	20	Sm – $Ia\bar{3}d$
	6	9	21	$Ia\bar{3}d$
	6	10	22	$Ia\bar{3}d$
	6	12	24	$Ia\bar{3}d$
C	10	5	35	$I23$
	10	6	36	$I23$
	10	7	37	$I23$
	10	8	38	$I23$
	10	9	39	$I23$
	10	10	40	$I23$
	10	12	42	$I23$
	10	14	44	$I23$ – Tet_{bi} – $Ia\bar{3}d$
	10	16	46	$I23$ – Tet_{bi} – $Ia\bar{3}d$
	10	18	48	$I23$ – Tet_{bi} – $Ia\bar{3}d$
	10	20	50	$Ia\bar{3}d$

Overall, the sequence proceeds from lamellar to columnar phases via 3D networks. This sequence is related to the increase of inter-material dividing surface curvature, i.e. the increasing alkyl volume gradually encloses the molecular rafts of aromatic cores. Interestingly, if we focus on the cubic phases, we can identify a phase sequence of $Ia\bar{3}d$ – $I23$ – $Ia\bar{3}d$. The typical twist angles between neighboring rafts are ~7.3° for $Ia\bar{3}d$ of **B*m*/*n*** , ~7.7° for $I23$ and ~8° for $Ia\bar{3}d$ of **C*m*/*n***. Thus, for polycatenar molecules, the volume of alkyl chains controls the transition from lamellar

to columnar phase. The intermediate cubic phases are controlled by the twist angle of molecular rafts.

References

S1. V. Gortz and J. W. Goodby, *Chem. Commun.* 2005*,* 3262–3264.

S2. D. H. Wang, Z. Shen, M. Guo, S. Z. D. Cheng, and F. W. Harris, *Macromolecules* 2007, **40**, 889–900.

S3. M. Alaasar, M. Prehm, Y. Cao, F. Liu and C. Tschierske, *Angew. Chem. Int. Ed*., 2016, **128**, 320–324.

S4. X. Zeng, G. Ungar, *J. Mater. Chem. C*, 2020, **8**, 5389-5398.

S5. N. A. Clark, Xi Chen, J. E. Maclennan, M. A. Glaser 2022 arXiv 2208.09784.

S6. M. Alaasar, S. Poppe, Y. Cao, C. Chen, F. Liu, C. Zhu and C. Tschierske, *J. Mater. Chem. C*, 2020, **8**, 12902-12916.

S7. M. Alaasar, Y. Cao, Y. Liu, F. Liu and C. Tschierske, *Chem. Eur. J*, 2022, **28**, e202201857.

S8. Y. Cao, M. Alaasar, L. Zhang, C. Zhu, C. Tschierske and F. Liu, *J. Am. Chem. Soc.*, 2022, **144**, 6936-6945.